Effect of Polyacriontrile (PAN) Concentration on Characteristics and Performance of TiO_2/N719/PAN-rGO for Dye-Sensitized Solar Cells

Herlin Pujiarti[1,2(✉)], Anjar Nur Ramadhani[1], Nabila Hari Arimbi[1], Markus Diantoro[1,2], Arif Nur Afandi[3], and Nasikhudin[1,2]

[1] Departement of Physics, Faculty of Mathematics and Natural Sciences, State University of Malang, Jl. Semarang No. 5, Malang 651145, Indonesia
herlin.pujiarti.fmipa@um.ac.id

[2] Center of Advanced Materials for Renewable Energy (CAMRY), State University of Malang, Jl. Semarang, No. 5, Malang 651145, Indonesia

[3] Departement of Electrical Engineering, Faculty of Engineering, State University of Malang, Malang 65145, Indonesia

Abstract. The increase in energy demand and reduced energy reserve, other alternative energy sources that are more environmentally friendly are needed, one of which is solar cells. Among several types of solar cells, Dye Sensitized Solar Cell is a type of solar cell that can produce electricity more efficiently. One of the ways to optimize DSSC efficiency is by modifying the counter electrode. PAN and rGO were selected and investigated for their characteristics because they can potentially develop high-efficiency DSSCs. The PAN-rGO counter electrode was prepared by screen printing with various PAN 5%, 10%, and 15% against therphinol solvent and characterization of the structure, morphology, optical properties, and DSSC efficiency using XRD, SEM-EDX, UV-Vis, and solar simulator I-V. The analysis results confirmed that increasing the concentration of PAN decreased crystal size and reduced particle size distribution and band gap values. The sample's highest efficiency value was recorded at a PAN concentration of 15%, which is 1.47% in the wavelength range of 325 nm with band gap energy of 3.83eV and particle size distribution of 162.15 nm. This result shows that PAN-rGO as a counter electrode can successfully be applied to DSSC.

Keywords: DSSC · PAN · rGO · Counter Electrode

1 Introduction

Energy is crucial in meeting human needs, which are increasing over time, so energy availability, especially from fossils, will be increasingly depleted. To overcome these problems, alternative energy is needed from other sources, including solar cell energy [1, 2]. Based on its development, solar cells are divided into three generations: silicon-based solar cells, thin-film-based solar cells, and Dye-Sensitized Solar Cells.

A. Doyan et al. (Eds.): ICSES 2022, APR 8, pp. 74–85, 2023.
https://doi.org/10.2991/978-94-6463-232-3_9

DSSC has several advantages, including having a low price, being easy to fabricate, being flexible, and having a high-efficiency performance [3, 4]. Researchers have paid close attention to the various potentials of the DSSC to conduct intensive research, resulting in rapid developments in the performance of the DSSC [5, 6]. DSSC consists of five main components, namely a metal oxide semiconductor superimposed on a conductive substrate (FTO), a photoanode, a dye attached to a metal oxide semiconductor (dye), and a redox pair electrolyte and a counter-electrode which are very important in determining the efficiency.

The counter electrode is one of the important components in the DSSC regulation process. It acts as a mediator for the electrolyte reduction process after the oxidation reaction of the dye with the electrolyte [7]. Platinum (Pt) is the most frequently used material for counter electrodes because of its electrocatalytic activity and high-efficiency results [8, 9]. However, Pt is an expensive and limited material [10]. Then another material is needed to replace Pt; namely, PAN composited with rGO, where the orbitals in PAN–rGO will overlap each other so that electron excitation can occur repeatedly to suppress recombination and good catalysis [11–13].

Research using materials NiS-rGO, rGO-NiCo2S4, PAN-CoS, rGO(3DGNs), and CoNi2S4 as Counter Electrode showed DSSC efficiency reached, respectively 9.5%, 8.15%, 7.41%, 9.79%, 9.22% [14–18]. In addition, the metal oxide TiO2 is attractive when combined with PAN-rGO because it can increase electron transport, which quickly reduces charge recombination so that it can increase the value of the current generated by solar cells [19]. This study aims to determine the effect of the concentration of PAN-rGO as a counter electrode on the structure, morphology, absorbance, and efficiency of DSSC. So far, many studies have not been on DSSC with PAN-rGO as a counter electrode. Therefore, research on the effect of PAN concentration on the characteristics and performance of TiO2/N719/PAN-rGO-based DSSCs needs to be done.

2 Method

2.1 DSSC Fabrication

Making DSSC begins with cleaning the FTO glass substrate with ethanol and then soaking it in soap and demineralized water for 15 min each. After that, the cleaned FTO glass was coated with mesoporous BL/TiO2 using a spin coating method with a speed of 3000 rpm and T-61 screen printing and then heated to 500 °C each. Then soaked in Dye N719 for 24 h. Preparation of 0.7 mM Dye N719 was produced from 0.0085 g and 10 mL of ethanol pa, which was dissolved at 300 rpm for 3 h. The TiO2 film was dyed in the dark for 24 h and then connected to a temperature of 500 °C for 30 min.

The synthesis of PAN/rGO was started by grinding PAN/rGO using a mortar with several variations of PAN concentration (5%, 10%, and 15% of the solvent) and 2 mg rGO mass for 30–60 min and then dripped with therphinol to make a paste (homogeneous). PAN-rGO as a paste was coated onto FTO using the screen printing method and then sintered at 100 °C to 400 °C for 15 min each. The layers are arranged to form a DSSC device and dripped from TDE mosalyte electrolyte to be tested I-V (Fig. 1).

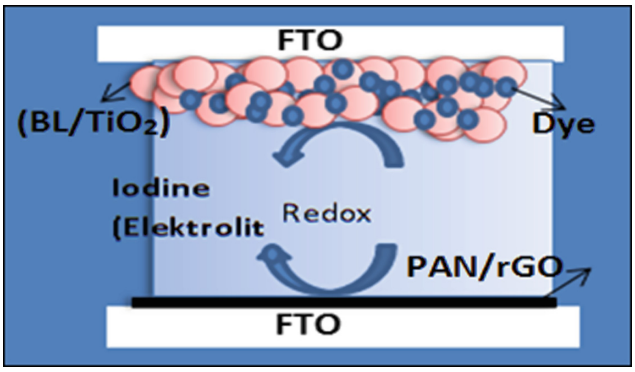

Fig. 1. Sandwich Structure for Dye-Sensitized Solar Cells

2.2 Characterization

Structural characterization was done using XRD to determine grain size, crystallinity, and crystal structure. Characterization of SEM mapping to determine the surface morphology and the distribution of nanoparticles and EDX to detect elements contained in the sample. UV-Vis characterization to determine optical properties. The conductivity material was obtained using the IV-2 probe test set to determine parameters such as Isc, FF, Jsc, and Voc so that the efficiency value of the DSSC will be obtained later.

2.3 Data Analysis

To analyze the crystal structure of the XRD results using the Rietica application and then refinement. Data processing using the Debye Scherrer equation in Eq. (1)

$$D = \frac{k\lambda}{\beta\cos\theta_\beta} = \frac{k\lambda}{FWHM\,(rad) \times \cos\theta_\beta} \tag{1}$$

There D is the crystal size, k is the Scherrer constant (0.9), λ the wavelength of the light (0.15406 nm), FWHM and angle percentage.

To determine the morphology obtained from the results of SEM-EDX characterization. The process of data analysis is done using *ImageJ* software and OriginPro8 software.

UV-Vis characterization produces a graph of the relationship between $(\alpha hv)^2$ and hv with a band gap to get the band gap value of the film sample used. Band gap will be calculated based on Eq. (2) for direct and Eq. (4) for indirect [20].

$$\alpha hv = A(hv - E_g)^{1/2} \tag{2}$$

$$\alpha hv = A(hv - E_g)^2 \tag{3}$$

With α absorption coefficient, hv is the photon energy, A is Constanta, and E_g is the *Band gap*.

The results of the I-V characterization obtained the current-voltage and power-voltage curves of the samples from the synthesis. By using Eq. (5), solar cell efficiency is obtained

$$FF = \frac{V_m I_m}{V_{OC} I_{SC}} \tag{4}$$

Obtained solar cell efficiency

$$\eta = \frac{P_{out}}{P_{in}} = \frac{V_{OC} I_{SC} FF}{FF}$$

$$\eta = \frac{V_m I_m}{SF} \tag{5}$$

3 Result and Discussion

3.1 PAN-rGO Structure Crystal from XRD

XRD characterization is used to analyze the structure, size, and phase of the crystals formed in a material. In XRD characterization, the Cu-Kα wave has a wavelength of 1.54060 with a diffraction angle range between 10–90°. The results of X-ray diffraction characterization in the form of a graph of the diffraction pattern on PAN nanocomposites with rGO concentrations between 5, 10, and 15% can be seen in Fig. 2.

The diffraction pattern formed is dominated by an amorphous arrangement showing activated carbon (rGO) structure. The diffraction peaks of rGO are shown at angles $2\theta = 24.50°$ and 44.88° with the hkl planes (002) and (100) [21, 22]. Besides, the diffraction peak at an angle of $2\theta = 17.02°$ with the hkl plane (110) shows the diffraction peak of PAN [23, 24]. In the three thin film samples with concentrations between 5, 10, and 15%, the diffraction peaks of the material were not very visible.

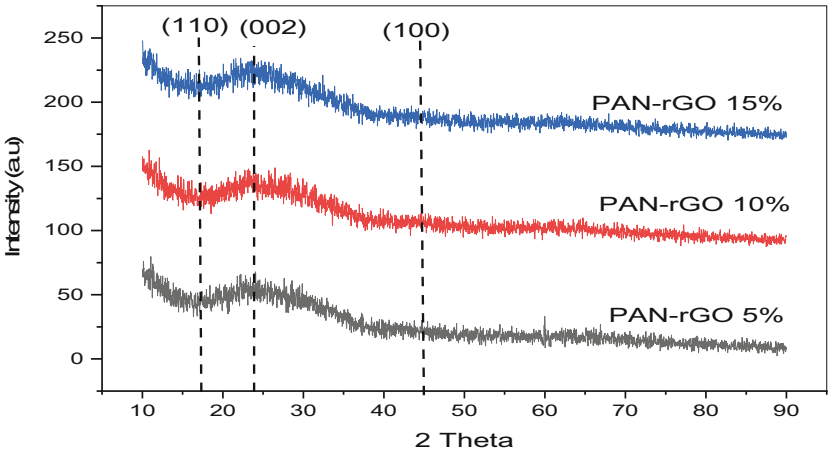

Fig. 2. The Result XRD PAN-rGO

Table 1. Crystal Size

Sample	FWHM (rad)	2 θ (°)	Crystal Size
PAN-rGO 5%	0,00542	24,55	26,18
PAN-rGO 10%	0,00546	24,68	25,91
PAN-rGO 15%	0,00558	24,86	25,44

From the results of data analysis to determine the crystal size by entering the FWHM and values in Eq. (1), the crystal size in PAN-rGO can be seen in Table 1.

The crystal grain size is at a concentration of 15% at 25, 44 nm, and the largest is at 5% at 26, 18 nm. This indicates that increasing the concentration of PAN decreases the crystal size.

3.2 Morphology from Results SEM

The morphology of the PAN-rGO counter electrode and its distribution can be observed in Fig. 2. SEM took the surface area of the PAN-rGO counter electrode with a magnification of 50,000x. A PAN-rGO counter electrode micrograph revealed an irregular shape and agglomeration (collection of elements in one point). From SEM, it can be seen that the concentration of 5% PAN in sheet form is higher than other PAN concentrations. From the Figure, it can be seen that the PAN-rGO composite can cause clumping in the sample. Clumps (also called aggregation) can appear because when mixing rGO with PAN using terpineol as a solvent and the wet mixing process that may occur does not take place evenly. As a result of this phenomenon, particles that have the same charge will most likely gather into one group. The analysis results were initiated by the study reported by [25]. Figure 3, shows the porosity value of PAN-rGO composite, whereas the PAN concentration increases, the porosity value decreases.

The particle size distribution and porosity can be seen in Table 2.

The analysis of the EDX results showed the percentage by weight and percentage of atomic phases contained in the PAN-rGO film sample shown in Fig. 4, where the most absent were C, N, and O.

3.3 The Optical Properties from UV-Vis Characterization

The optical properties of PAN/rGO were characterized using a UV-Vis spectrophotometer. The light absorbed at a certain wavelength is related to the energy required for electrons to excite from the valence band to the conduction band [26]. Figure 5. Shows absorbance and wavelength range of PAN-rGO. The band gap value is related to the electrical conductivity produced; the greater the conductivity value, the smaller the band gap value [27, 28]. The value of the band gap can be analyzed using the Tauc Plot method

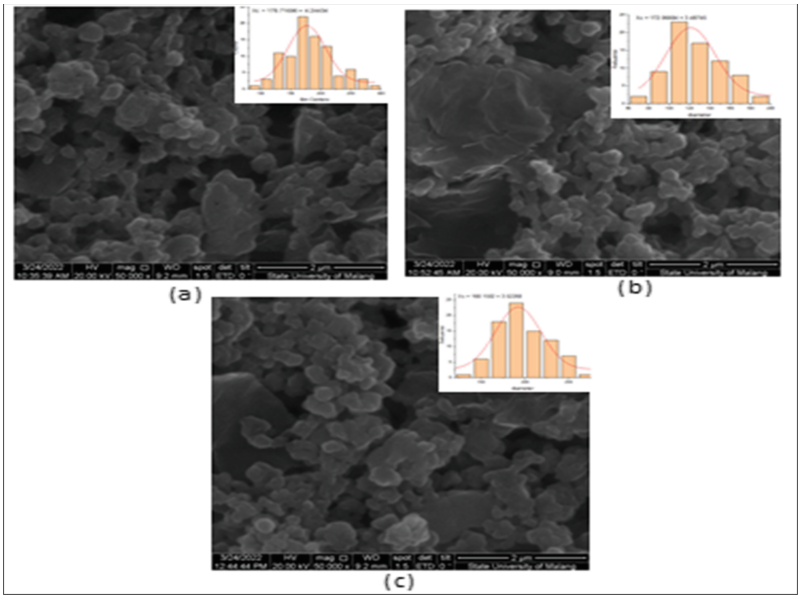

Fig. 3. Morphology of PAN-rGO and Particle Distribution at PAN concentrations (a) 5% (b) 10% and (c) 15%

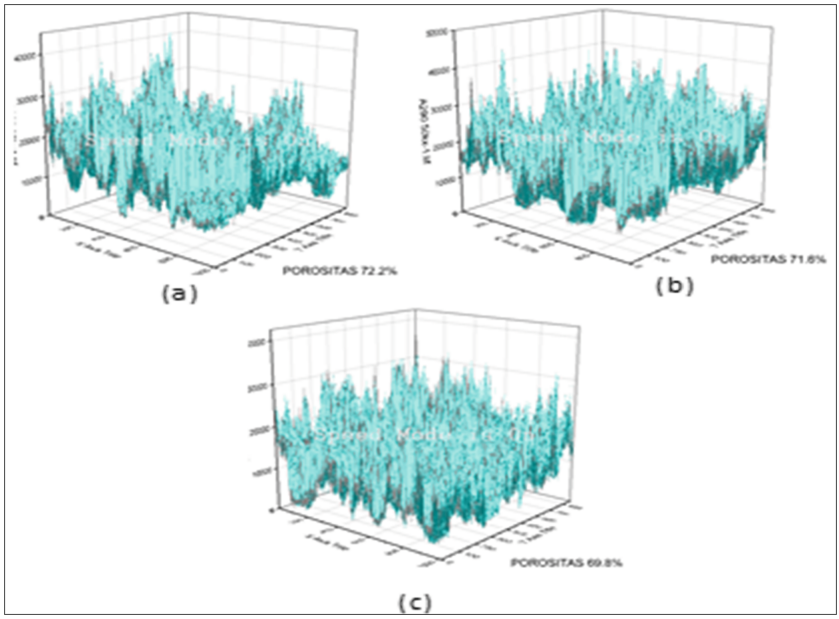

Fig. 4. Porosity value of PAN-rGO at PAN concentrations (a) 5%, (b) 10%, and (c) 15%

Table 2. Distribution of mean particle size and porosity

Concentration PAN	Distribution of mean particle (nm)	Porosity (%)
5%	178,78	72,2
10%	172,06	71,8
15%	168,15	69,8

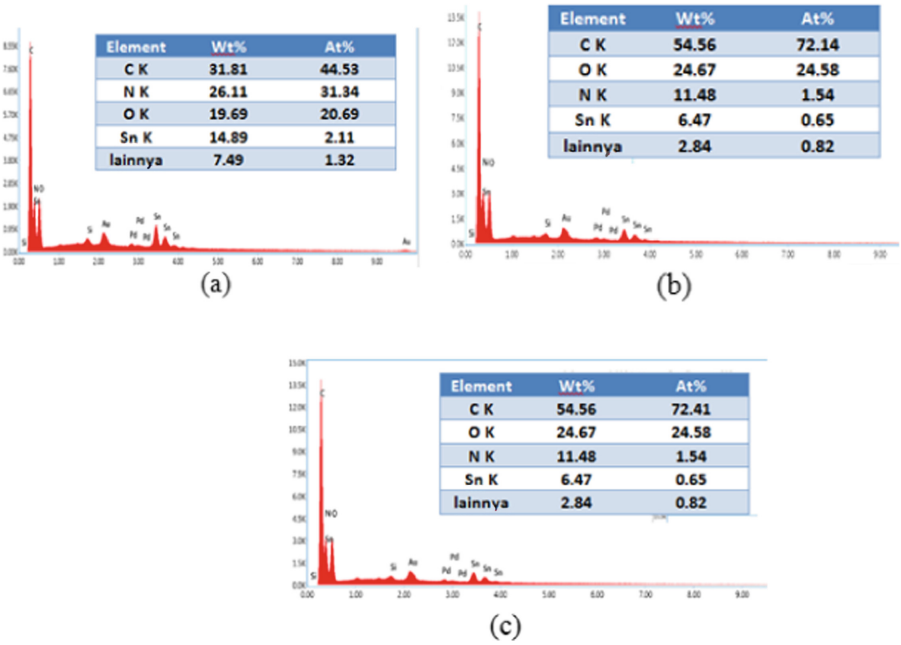

Fig. 5. PAN-rGO EDX results at concentrations of PAN (a) 5%, (b) 10%, (c) 15%

by making hv and (αhv) 1/2 curves. The maximum absorbance occurs at a wavelength of 325 nm, indicating a band gap energy of 3.83 eV.

Band gap values are presented in Table 3.

In previous studies, the value of the PAN band gap reached 3.92 eV [29], while the band gap value for rGO ranged from 1.4–3.3 eV [30]. Figure 6 shows that adding PAN mass can reduce the value of the PAN-rGO band gap. The band gap value of rGO increased after being composited with PAN.

3.4 DSSC Efficiency from I-V Characterization

The photovoltaic properties of TiO_2/N719/PAN-rGO devices were tested using a solar simulator I-V to get the efficiency value of light conversion into electrical energy. The DSSC system consists of a TiO_2 semiconductor composite material as a photoanode with N719 dye as a dye and PAN-rGO as a Counter Electrode connected to a single

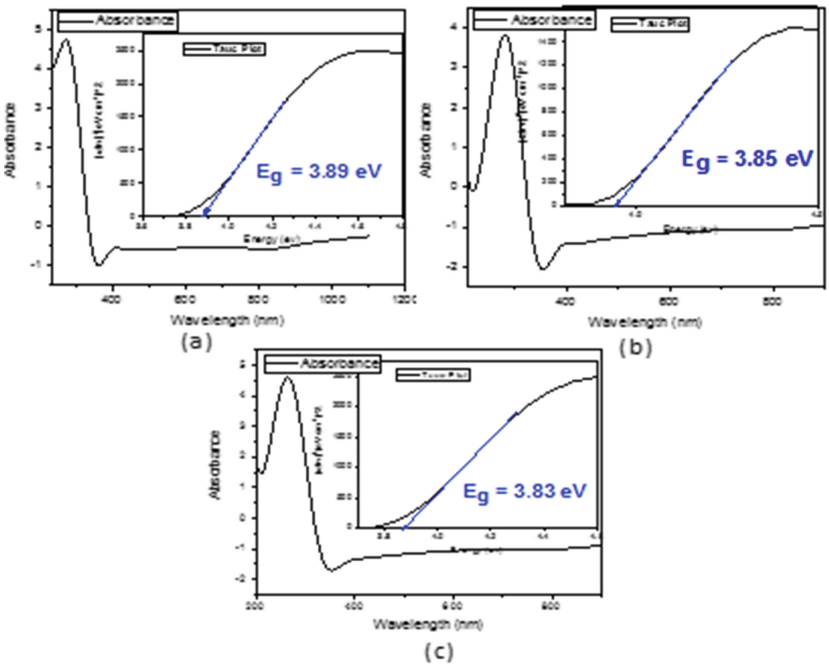

Fig. 6. Absorbance and band gap energy of PAN-rGO at PAN concentrations (a) 5%, (b) 10% and (c) 15%

Table 3. Band gap values of PAN-rGO with variations in the concentration of PAN.

Concentration PAN	Energy gap (eV)
5%	3,89
10%	3,85
15%	3,83

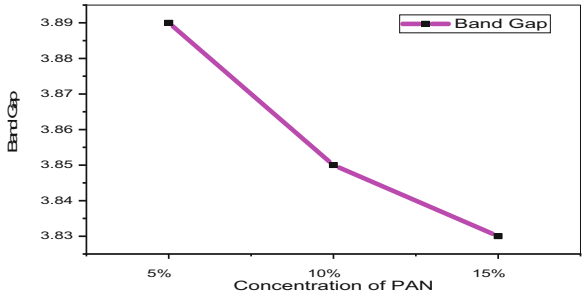

Fig. 7. Shows the relationship between PAN concentration and band gap

diode circuit which is illuminated by a xenon lamp with an intensity of 100 mW/cm^2. Efficiency is measured in a geometric area of 0.25 cm^2.

The following are the characteristic IV parameters which are shown in Table 4.

Based on the results of the I-V test through characterization using a solar simulator, the efficiency values for each concentration of PAN 5%, 10%, and 15%, respectively, were 1.25; 1.28; and 1.47%. The highest efficiency value was found at PAN concentration of 15%, which was 1.47% and Jsc of 8.92 mA/cm^2, which was related to the crystal size, morphology, and absorbance values possessed by these concentrations. At 15% PAN concentration, the smallest crystal size is 23.37 nm; in the morphological structure, there is less agglomeration so the smallest grain size distribution is 162.15 nm, and the porosity is 63% the smallest. The efficiency of the device at PAN concentration of 15% showed optimum results; this indicates that the recombination rate in the system is quite low. Figure 7(a). Shows I-V DSSC curves for all PAN-rGO concentrations, which shows that increasing the concentration of PAN can increase the efficiency of PAN-rGO as shown in Fig. 7(b). Efficiency value increases after composite (Fig. 8).

Table 4. Characteristic IV parameters

Sample	I_{sc} mA	V_{oc} (V)	J_{sc} (mA/cm^2)	FF	η (%)
PAN-rGO 5%	2,25	0,58	9,02	0,24	1,25
PAN-rGO 10%	2,03	0,62	9,30	0,22	1,28
PAN-rGO 15%	2,32	0,61	8,92	0,27	1,47

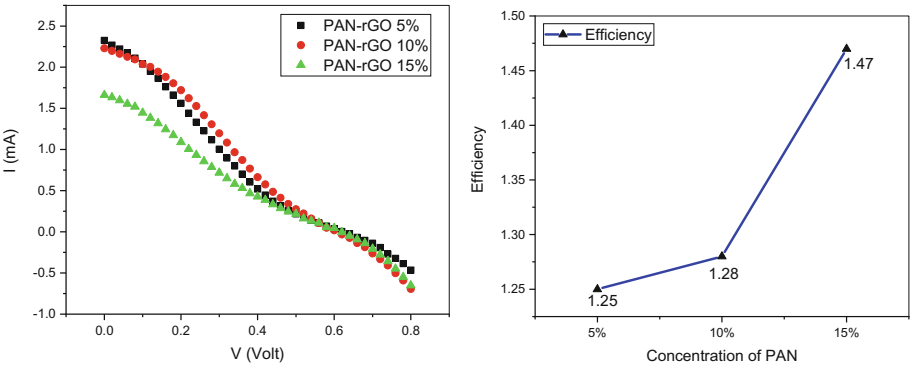

(a) (b)

Fig. 8. Shows I-V (a) DSSC curves for all PAN-rGO concentrations and (b) the relationship between PAN concentration and efficiency.

4 Conclusions

PAN-rGO counter electrodes with various PAN concentrations have been identified. Increasing the concentration of PAN in the solvent caused the crystal size to decrease to 25, 44 nm. The morphology of PAN-rGO has irregular shapes, agglomeration occurs (collection of elements in one point), and the particle size distribution decreases with increasing PAN concentration values reaching 162.15 nm. Increasing the concentration of PAN reduces the band gap value to 3.83 eV because the smallest grain size can expand the counter electrode, so the electrical conductivity produced is quite high. High electrical conductivity causes more electrons to be converted into electrical energy, so the efficiency value obtained is quite high. The optimum efficiency value at 15% PAN concentration is 1.47%. Based on the results of this study, it is proven that PAN-rGO can be applied to DSSC based on BL/TiO2/N719/Electrolyte/PAN-rGO although the resulting efficiency is less than optimal.

Acknowledgments. This research was gratefully supported by a research grant from PNBP through Universitas Negeri Malang from the Ministry of Research, Technology, and Higher Education, Indonesia.

References

1. M. I. Darmawan and A. Supriyanto, "Pengaruh Konsentrasi Ruthenium (N719) sebagai Fotosensitizer dalam Dye-Sensitized Solar Cells (DSSC) Transparan," pp. 104–108, 2016.
2. F. Hidayanti, Buku Ajar Aplikasi Sel Surya, vol. 6, no. 11. 2020.
3. D. Wei, "Dye sensitized solar cells," Int. J. Mol. Sci., vol. 11, no. 3, pp. 1103–1113, 2010, https://doi.org/10.3390/ijms11031103.
4. M. Chen and L. Shao, "Review on the recent progress of carbon counter electrodes for dye-sensitized solar cells," Chem. Eng. J., vol. 304, pp. 629–645, 2016, https://doi.org/10.1016/j.cej.2016.07.001.
5. B. O'Regan and M. Grätzel, "A low-cost, high-efficiency solar cell based on dye-sensitized colloidal TiO2 films," Nature, 1991, https://doi.org/10.1038/353737a0.
6. K. Kakiage, Y. Aoyama, T. Yano, K. Oya, J. Fujisawa, and M. Hanaya, "Highly-efficient dye-sensitized solar cells with collaborative sensitization by silyl-anchor and carboxy-anchor dyes," Chem. Commun., vol. 51, no. 88, pp. 15894–15897, 2015, https://doi.org/10.1039/C5CC06759F.
7. Fatiatun, "Performance Counter Electrode (CE) Made of Reduced Graphene Oxide (rGO) For Dye Sensitized Solar Cells (DSSCs) Applications," 2018. https://warstek.com/ce/.
8. G. Yue et al., "Platinum/graphene hybrid film as a counter electrode for dye-sensitized solar cells," Electrochim. Acta, vol. 92, pp. 64–70, Mar. 2013, https://doi.org/10.1016/j.electacta.2012.11.020.
9. P. Raghavan, J. Manuel, X. Zhao, D. S. Kim, J. H. Ahn, and C. Nah, "Preparation and electrochemical characterization of gel polymer electrolyte based on electrospun polyacrylonitrile nonwoven membranes for lithium batteries," J. Power Sources, vol. 196, no. 16, pp. 6742–6749, 2011, https://doi.org/10.1016/j.jpowsour.2010.10.089.

10. J. Gong, J. Liang, and K.Sumathy, "Review on dye-sensitized solar cells (DSSCs): Fundamental concepts and novel materials," Renew. Sustain. Energy Rev., vol. 16, no. 8, pp. 5848–5860, Oct. 2012, https://doi.org/10.1016/j.rser.2012.04.044.
11. Safriani, Lusi, A. Chintia, C. Suryaningsih, and A. Sri Aprilia, "Effect Of Additional rGO On TiO2 Photoanodes On Dye-Sentitized Solar Cell Performance," vol. 11, no. 01, pp. 1–7, 2021.
12. A. Pratama, L. Destiarti, and A. Adhitiyawarman, "Synthesis of Titanium Oxide/Reduced Graphene Oxide (TiO2/rGO) for Photocatalysis of Methylene Blue Dyes," Positron, vol. 11, no. 1, p. 31, 2021, https://doi.org/10.26418/positron.v11i1.45355.
13. F. W. Low, C. W. Lai, K. M. Lee, and J. C. Juan, "Enhance of TiO2 dopants incorporated reduced graphene oxide via RF magnetron sputtering for efficient dye-sensitized solar cells," Rare Met., vol. 37, no. 11, pp. 919–928, Nov. 2018,https://doi.org/10.1007/s12598-018-1064-4.
14. A. Sarkar, A. K. Chakraborty, and S. Bera, "NiS/rGO nanohybrid: An excellent counter electrode for dye sensitized solar cell," Sol. Energy Mater. Sol. Cells, vol. 182, pp. 314–320, Aug. 2018, https://doi.org/10.1016/j.solmat.2018.03.026.
15. K. S.Anuratha, M. Ramaprakash, S. K. Panda, and S. Mohan, "Studies on synergetic effect of rGO-NiCo2S4 nanocomposite as an effective counter electrode material for DSSC," Ceram. Int., vol. 43, no. 13, pp. 10174–10182, Sep. 2017, https://doi.org/10.1016/j.ceramint.2017.05.042.
16. V. Murugadoss, S. Arunachalam, V. Elayappan, and S. Angaiah, "Development of electrospun PAN/CoS nanocomposite membrane electrolyte for high-performance DSSC," Ionics (Kiel)., vol. 24, no. 12, pp. 4071–4080, Dec. 2018, https://doi.org/10.1007/s11581-018-2540-4.
17. B. Tang et al., "Three-dimensional graphene networks and RGO-based counter electrode for DSSCs," RSC Adv., vol. 9, no. 28, pp. 15678–15685, 2019, https://doi.org/10.1039/C9RA02792K.
18. A. Sarkar, S. Bera, and A. K. Chakraborty, "CoNi2S4-reduced graphene oxide nanohybrid: An excellent counter electrode for Pt-free DSSC," Sol. Energy, vol. 208, no. October 2019, pp. 139–149, 2020, https://doi.org/10.1016/j.solener.2020.07.075.
19. F. Yuliasari, V. Marcelina, L. Safriani, U. Padjadjaran, A. Aprilia, and N. Sciences, "Manufacture of Dye Sensitized Solar Cells with Graphene Oxide as Diffuse Material for TiO2 Photoanodes," no. 2784, 2019, https://doi.org/10.24198/jmei.v8i2.19900.
20. M. Diantoro, T. Suprayogi, A. Taufiq, A. Fuad, and N. Mufti, "The Effect of PANI Fraction on Photo Anode Based on TiO2-PANI /ITO DSSC with β-carotene as Dye Sensitizer on its Structure, Absorbance, and Efficiency," Mater. Today Proc., vol. 17, pp. 1197–1209, 2019, https://doi.org/10.1016/j.matpr.2019.05.345.
21. N. M. S. Hidayah et al., "Comparison on graphite, graphene oxide and reduced graphene oxide: Synthesis and characterization," 2017, p. 150002, https://doi.org/10.1063/1.5005764.
22. X.Qiao, S. Liao, C. You, and R. Chen, "Phosphorus and Nitrogen Dual Doped and Simultaneously Reduced Graphene Oxide with High Surface Area as Efficient Metal-Free Electrocatalyst for Oxygen Reduction," Catalysts, vol. 5, no. 2, pp. 981–991, Jun. 2015, https://doi.org/10.3390/catal5020981.
23. H. S. Mahmood and M. K. Jawad, "Antibacterial activity of chitosan/PAN blend prepared at different ratios," 2019, p. 020078, https://doi.org/10.1063/1.5138564.
24. H.-Y. Liu, L. Xu, and Q.-L. Sun, "Highly aligned electrospun nanofibers by hot-drawing," Therm. Sci., vol. 19, no. 4, pp. 1357–1360, 2015, https://doi.org/10.2298/TSCI1504357L.
25. A. S.AlShammari, M. M. Halim, F. K. Yam, and N. H. M. Kaus, "Synthesis of Titanium Dioxide (TiO2)/Reduced Graphene Oxide (rGO) thin film composite by spray pyrolysis technique and its physical properties," Mater. Sci. Semicond. Process., vol. 116, no. December 2019, p. 105140, 2020, https://doi.org/10.1016/j.mssp.2020.105140.

26. M.Caglar, S. Ilican, and Y. Caglar, "Influence of dopant concentration on the optical properties of ZnO: In films by sol–gel method," Thin Solid Films, vol. 517, no. 17, pp. 5023–5028, Jul. 2009, https://doi.org/10.1016/j.tsf.2009.03.037.
27. P. Tyas, "Determination of Tire Gap and Conductivity of Sn(S0,8Te0,2) and Sn(S0,6Te0,4) thin films," Universitas Negeri Yogyakarta, 2017.
28. M. Rani and S. K.Tripathi, "Fabrication, Characterization and Photoconducting Behaviour of Mesoporous ZnO, TiO 2 and TiO 2 /ZnO Bilayer System: Comparative Study," Energy Environ. Focus, vol. 2, no. 3, pp. 227–234, Sep. 2013, https://doi.org/10.1166/eef.2013.1055.
29. T. Tański, W. Matysiak, and B. Hajduk, "Manufacturing and investigation of physical properties of polyacrylonitrile nanofibre composites with SiO 2 , TiO 2 and Bi 2 O 3 nanoparticles," Beilstein J. Nanotechnol., vol. 7, pp. 1141–1155, Aug. 2016, https://doi.org/10.3762/bjnano.7.106.
30. S. L. Joseph, A. O. John, F. K. Mugwang, and G. G. Katana, "Tuning the Band Gap Energy of Reduced Graphene Oxide Using Biopolymer Chitosan for High Power and Frequency Device Applications," vol. 7, no. 1, pp. 1–12, 2019.